analytical chemistry

pubs.acs.org/ac Article

A FLIM Microscopy Based on Acceptor-Detected Förster Resonance Energy Transfer

Roberto F. Delgadillo,* Katie A. Carnes, Kathia Zaleta-Rivera, Omar Olmos, and Lawrence J. Parkhurst*

Cite This: *Anal. Chem.* 2021, 93, 4841−4849 Read Online

ACCESS | Metrics & More | Article Recommendations | Supporting Information

ABSTRACT: Time-resolved donor-detected Förster resonance energy transfer (trDDFRET) allows the observation of molecular interactions of dye-labeled biomolecules in the ∼10−100 Å region. However, we can observe longer-range interactions when using time-resolved acceptor-detected FRET (trADFRET), since the signal/noise ratio can be improved when observing the acceptor emission. Therefore, we propose a new methodology based on trADFRET to construct a new fluorescence lifetime microscopy (FLIM-trADFRET) technique to observe biological machinery in the range of 100−300 Å in vivo, the last frontier in biomolecular medicine. The integrated trADFRET signal is extracted in such a way that noise is canceled, and more photons are collected, even though trADFRET and trDDFRET have the same rate of transfer. To assess our new methodology, proof of concept was demonstrated with a set of well-defined DNA scaffolds.

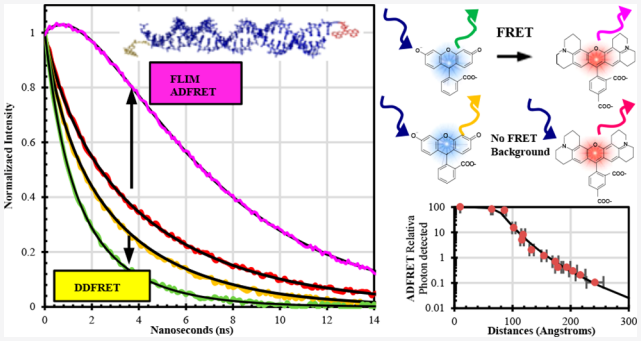

1. INTRODUCTION

Macromolecular assemblies are responsible for replication, transcription, translation, vesicular transport, viral, and parasitic infections.[1−6] Fortunately, after the elucidation of these macromolecular mechanisms, new therapeutic approaches can be created to better fight disease by repairing, halting degenerative processes, or stopping infectious machinery at the molecular level.[4,7,8] The latest microscopy technologies give molecular resolution below 300 Å (Figure 1A, orange box) and the current "fluorescence lifetime imaging microscopy" based on time-resolved donor-detected Förster resonance energy transfer (FLIM-trDDFRET) methodology (Figure 1A, yellow box)[2] can observe molecular activities in the 10−100 Å range. Traditional trDDFRET lifetime of D in the presence of A ($\tau_{D(A)}$) gets closer to the reference donor lifetime (τ_D) at increasing D-A distances.

In this work, we present the equations and experimental strategies to observe trFRET-sensitized acceptor (A), creating the basis of a new type of FLIM, herein called FLIM-trADFRET, that increases the FRET resolution up to 300 Å (Figure 1A−D, Database S1). For trDDFRET and trADFRET, the rate of transfer (k_t) and the FRET efficiency is the same in both cases (Figure 1E−J),[9−16] but the latter has unlimited photon accumulation and background noise reduction (red line, Figure 1G,H) allowing better signal−noise ratio (S/N)[17] (Figure 1K,L). Our new approach is based on the photon accumulation of the trADFRE $\langle \tau^{Obs}_{trADFRET} \rangle$ over a reference lifetime $\langle \tau_{Std} \rangle$ that has been acquired with a standard solution (Figure 1J,K). Therefore, our FLIM-trADFRET accumulate signals like ^1H and ^{13}C NMR experiments, where nuclei relaxation is averaged in low-concentration samples.[18,19] Similarly, magnetic resonance imaging (MRI) in which T1 and T2 relaxations are collected by stacking image frames to improve resolution[20−22] or for stealth airplane detection in the military.[23]

2. MATERIALS AND METHODS

The single- and double-labeled *N′* and *N* oligo series (Figure S1, Table 1) were synthesized with their corresponding unlabeled complementary strands by TriLink Biotechnologies, Inc. (San Diego, CA) followed by both HPLC and PAGE purification. All experiments were conducted at 20 ± 0.1 °C in 10 mM Tris, 100 mM KCl, 2.5 mM $MgCl_2$ and 1 mM $CaCl_2$ (pH 8). The top strand concentrations were 10−50 nM, and duplexes were formed with 10× complement concentration.

2.1. Instrumentation, Data Acquisition, and Fitting Analysis. Time-resolved decays were collected by two instruments: (1) LaserStrobe, LS (Photon Technologies, Inc., Birmingham, NJ) with 10 Hz excitation rate provided with a PLD481 dye tuned to 481 nm with emission collected through nonfluorescing 520 and 620 nm interference filter (10BPF10-520 and 10BPF10-620, full width at half maximum (FWHM) = 9 nm, Oriel Corp., Stratford, CT) preceded by a 50 mm × 50

Received: October 23, 2020
Accepted: February 1, 2021
Published: March 10, 2021

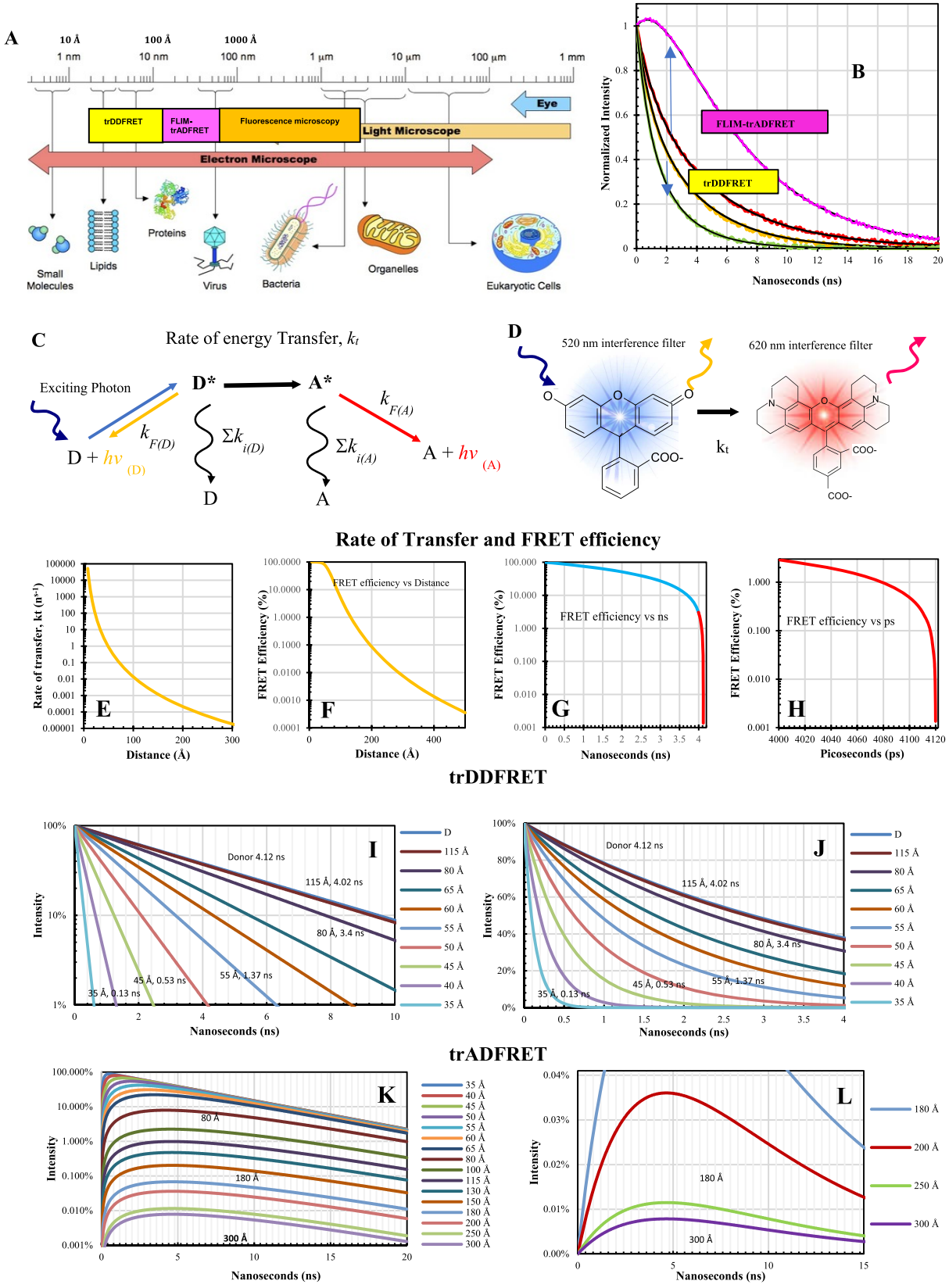

Figure 1. (A) Scale of living organisms (www.microbiologyinfo.com). Fluorescence microscopy techniques (orange box) have breached Abbe's limit and reached ~300 Å resolution. Traditional trDDFRET (yellow box) for our FRET pairs detect molecular interaction in the 10−100 Å region (yellow box). However, our FLIM-trADFRET methodology (pink box) can detect macromolecular interaction in the remaining gap region of 100 Å−300 Å. (B) The sensitized trADFRET intensity (purple, $I_{trADFRET}$) has approximately threefold higher intensity with respect to its lifetime reference $\langle\tau_{Std}\rangle$ (red) than the traditional trDDFRET (green, $\tau_{D(A)}$) and its respective reference (orange, τ_D) (Database S1). (C) The FRET process initiates by an excitation pulse (blue) that excites D toward D*, which transfers its energy in the presence of an acceptor (A). The kinetic mechanism is $a \rightarrow b \rightarrow c$ with

https://dx.doi.org/10.1021/acs.analchem.0c04492
Anal. Chem. 2021, 93, 4841−4849

Figure 1. continued

some branches (black arrows), where a and b correspond to D* and A*, respectively, and c corresponds to the photons, $h\nu_{(A)}$, emitted by the excited A*. The value of d[A*]/dt, is 0 at t_0, and it rises to a maximum (t_{max}) and decays exponentially to 0. D* and A* are inactivated via their respective radiative lifetimes (τ), that is, the sum of the reciprocal of the sum fluorescence rate and the nonradiative pathways (Σk_i, black arrows). (D) The fluorescein (Fl, donor) and x-rhodamine (Xr, acceptor) dyes have broad emissions (yellow and red arrows, respectively) for which signals are collected by 520- and 620-nm interference filters. The excitations were 481 and 470 nm for LaserStrobe and FluoTime, respectively. (E, F) k_t (Eq 4) and FRET efficiency ($100\% \times (1 - \tau_{D(A)}/\tau_D)$) plots as a function of mean interdye distance ($\overline{R}$) for the Fl_{int} and Xr pair attached to the N oligo series for which R_0 is 61.8 Å and τ_D is 4.12 ns (Database S2). (G, H) The k_t as a function of lifetimes in nanoseconds (ns) and picoseconds (ps), respectively. The $\tau_{D(A)}$ dropped 1.5 logs from 0 to 4 ns (blue), and 3 logs from 4.0 to 4.12 ns (red). The$\overline{R}$ of 115, 125, 180, and 300 Å correspond to $\tau_{D(A)}$ values of 4023, 4045, 4113, and 4119.7 ps, respectively, which corresponded to energy transfers of 2.35, 1.44, 0.164 and 0.008% in the same order (Database S1). (I, J) Simulated trDDFRET lifetimes, in logarithmic and percentage scale, respectively. τ_D is 4.12 ns, and $\tau_{D(A)}$ varies from 0.13, 1.37, 3.40, to 4.02 ns for $\overline{R}$ of 35, 55, 80, and 115 Å, respectively (Database S1). As the distance increases the lifetime difference, $\Delta\tau = \tau_D - \tau_{D(A)}$, approaches to zero thus making the $\overline{R}$ calculation impossible. Thus, at 115 Å, τ_D and $\tau_{D(A)}$ (blue and brown curve, respectively) cannot be discriminated by the fitting algorithms due to curve overlapping. (K, L) The FLIM-trADFRET simulations from 35 Å up to 300 Å; our methodology utilizes the time-resolved sensitized trADFRET whose rising curve allows photon accumulation over the steady background, $\langle\tau_{Std}\rangle$. For our dye pairs at distances beyond 100 Å, the trDDFRET $\tau_{D(A)}$ approaches to the τ_D, acting as a limiting maximum value. However, in the case of the trADFRET, the signal accumulates on top of the $\langle\tau_{Std}\rangle$ thus improving S/N ratio by increasing sensitized signal strength and decreasing background noise.

Table 1. N′ and N Oligo Sequences. The DNA Oligos Were Labeled with 5′ X-Rhodamine (5′-Xr*, Acceptor) and 3′ Fluorescein (3′-*Fl, Donor) Attached by 6-Carbon Long Linkers for the Former, and the Latter with 5′Xr and Internally Labeled Fl by a 12-Atom Long Linker (Fl_{int}, Donor)[a]

N′ series	double-labeled DNA sequences
14N′	5′-Xr*GGGAATAACTTGGC*Fl-3′
29 N′	5′-Xr*GGCTAATACTATATAATAGACGACTTGGC*Fl-3′
N series	double-labeled DNA sequences
24 N	5′-Xr*GCGAATAATAATGACGACTTGAA(dT-Fl_{int})GTGGC-3′
29 N	5′-Xr*GCGAATAATAATAACGTGACGACTTGAA(dT-Fl_{int})GTGGC-3′
34 N	5′-Xr*GCGAATAATAATAAATCGACGTGACGACTTGAA(dT-Fl_{int})GTGGC-3′
39 N	5′-Xr*GCGGCAATAGATAATATGAACTAATTTAACTACTTGAA(dT-Fl_{int})GTGGC-3′
44 N	5′-Xr*GCGGCATAGACTAATATTTTTATAACTAATTTAACTTCTTGAA(dT-Fl_{int})GTGGC-3′
49 N	5′-Xr*GGGAATAATAATAAAGGGAAGAAGACTTGGCTCGACGTGACGACTTGAA(dT-Fl_{int})GTGGC-3′
52 N	5′-Xr*GCGACAATAATAATAAAGGGAATAAGACTTGGCTCGACGTCACGACTTGAA(dT-Fl_{int})GTGGC-3′
56 N	5′-Xr*GCGTAGTGCTATGTAATCGACGAATCGGGCAAAGCTAGTAGTTAGTAAACTTGAA(dT-Fl_{int})GTGGC-3′
34 N complements	DNA sequences
standard	5′-GCC-ACA-TTA-AAG-TCG-TCA-C**G**T-CGA-TTT-ATT-ATT-ATT-CGC-3′
mismatch T at 20	5′-GCC-ACA-TTA-AAG-TCG-TCA-C**T**T-CGA-TTT-ATT-ATT-ATT-CGC-3′
mismatch A at 20	5′-GCC-ACA-TTA-AAG-TCG-TCA-C**A**T-CGA-TTT-ATT-ATT-ATT-CGC-3′
mismatch C at 20	5′-GCC-ACA-TTA-AAG-TCG-TCA-C**C**T-CGA-TTT-ATT-ATT-ATT-CGC-3′
d spacer (abasic) at 20	5′ GCC-ACA-TTC-AAG-TCG-TCA-C(**d Spacer**)T-CGA-TTT-ATT-ATT-ATT-CGC-3′
two d-spacers at 20−21	5′ GCC-ACA-TTC-AAG-TCG-TCA-(**d Spacer**)(**d Spacer**)T-CGA-TTT-ATT-ATT-ATT-CGC-3′
1st half (Flint side)	5′-GCC-ACA-TTC-AAG-TCG-TCA-C-3′
2nd half (Xr side)	5′-T-CGA-TTT-ATT-ATT-ATT-CGC-3′

[a]Also, the single-labeled D (DNA*Fl-3′ and DNA*Fl_{int}) and A (Xr*DNA) sequences were synthesized. The *N′* series was composed of only two sequences with a 14 and 29 basepair (bp) interdye separation; and in the case of the *N* oligos, they have an interdye separation of 29, 34, 39, 44, 49, 52, and 56 bps without considering the extra 5 bps toward the 3′end. The standard complements and several versions of 34 N complements were synthesized to hybridized with the top strands.

mm aperture and 1 cm path length quartz liquid filter of 24.1 mM acetate buffered dichromate, pH 4, to remove scattered excitation light. To collect direct A lifetime, the excitation was provided by a PLD575 dye tuned to 585 nm. The emission collection was carried out in 120−150 channels in a 23−25 ns window with three successive replicate decays collected and averaged to yield one sample decay. A total of four sets of six decays were collected for a total of 72 individual curves. The instrument response function (IRF) was obtained for each set using a diluted glycogen solution for deconvolution purposes (Database S3 and Database S5). (2) FluoTime, FT (PicoQuant GmbH, Berlin, Germany), with 20 MHz pulsed excitation rate at 470 nm provided by a pulsed diode laser LDH-P-C-470 (PicoQuant, GmbH, Berlin, Germany) with emission collected through the same filters. In the case of the FluoTime, the decays were collected at 20 MHz over 6 s with a photon detection rate below 1% of the excitation repetition frequency and concentrations maintained between 20 and 50 nM to avoid pile-up error. The IRF was collected every 30−60 min using a solution of colloidal silicon dioxide (LUDOX, DuPont, Wilmington, DE) with the baseline intensity matched to the sample decays to facilitate fitting, having an FWHM of 40 picoseconds (ps) or less. A total of 350 sample decays were collected in 50 sets of 7 decays each and at least 175 decays for the standard solutions grouped in 25 sets of 7 decays each (full data set provided, Database S3, Database S6, and Database S7).

The raw curves were fitted to mono-, bi-, and tri-exponential decay models evaluated by iterative deconvolution based on the Marquardt algorithm. In the case of the LaserStrobe, the optimal model was identified using χ^2, the runs test normal variate, *Z*,

https://dx.doi.org/10.1021/acs.analchem.0c04492
Anal. Chem. 2021, 93, 4841−4849

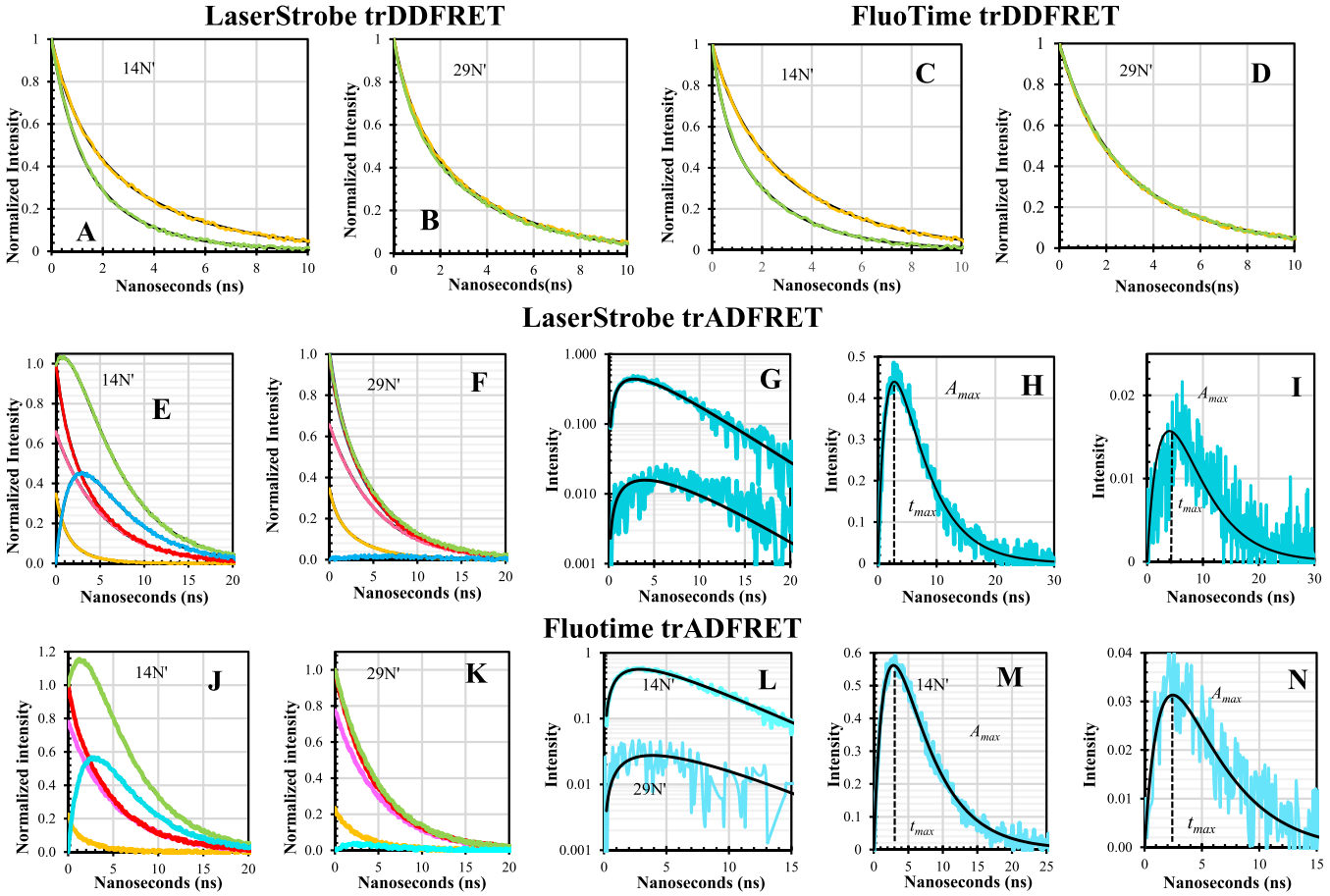

Figure 2. Time-resolved DDFRET and trADFRET lifetimes. Deconvoluted time-resolved intensity for the 14 N' (A, B) and 29 N' (C, D) in the absence (orange, $\overline{I}_D$) and presence of A (green, $\overline{I}_{D(A)}$) with 2% added noise and respective fits (τ_D and $\tau_{D(A)}$, black lines) for both instruments. In contrast to 14 N′, the 29 N′ overlapping curves and lifetimes impeded $P(R)$ calculations (Database S4). (E, F) The observed LaserStrobe trADFRET intensity (green, $\overline{S}_{trADFRET}$) with 2% added noise for the double-labeled 14 N' and 29 N' collected with the 620 nm interference filter at 481 nm excitation, respectively. The leaked D intensity in the presence of A (orange, $\overline{I}_{D(A)}$) corresponded to the trDDFRET decays (shown in figure A), is multiplied by $1/(r+1)$, and the directly excited A (pink, $\overline{I}_A$) is multiplied by $r/(r+1)$, where the "r" parameter is the $I_A/I_{D(A)}$ ratio (eq 11, Database S5). The $\overline{I}_{D(A)}$ and $\overline{I}_A$ were acquired with the same N oligo sample with the 520-nm filter at 481 nm excitation, and the 620 nm interference filter at 585 nm excitation wavelength, respectively. The sum of $\overline{I}_{D(A)}\cdot 1/(r+1) + \overline{I}_A\cdot r/(r+1)$, contaminating signals (red) were removed to extract the sensitized $I_{trADFRET}$ (light blue). The sensitized $I_{trADFRET}$ for the 14 N' and 29 N' with the least-squares fitted curve (black) in a logarithmic scale (G) and linear scale (H, I), respectively. (J–N) The sensitized $I_{trADFRET}$, $\overline{I}_{D(A)}$ and $\overline{I}_A$ of 14 N′ and 29 N′ acquired with FluoTime collected with the same filters but at 470 nm excitation (Database S6). The calculated $\overline{R}$ and σ values were equivalents for both instruments (Table 2).

and the Durbin–Watson parameter. In the case of the FluoTime instrumentation, only a global fitting χ^2 value is given for each set to discriminate models (Database S3, Database S6, and Database S7).

3. RESULTS AND DISCUSSION

3.1. Dye Spectroscopy Properties. Our testing material were two families of 5′end labeled *x*-rhodamine (Xr) and either 3′ end (3′-Fl) and internally labeled Fl (Fl_{int}) duplex DNA oligomers, called N' and N oligos, respectively (Table 1, Figure S1). We preferred DNA since it can be designed to have a well-defined straight and fixed geometry,[24,25] instead of a peptide scaffold as seen in earlier seminal work.[26] Our duplexes have been extensively studied in our previous trDDFRET work with two spectrometers (FluoTime and LaserStrobe) and we have characterized the in situ dye spectroscopy properties, such as maximum molar absorbances (ε), excitation ratios, absorption and emission spectra shifting, quantum yields (QY), natural lifetime (τ^0), nonstatically quenched fraction ($1-S$), dynamic lifetime (Φ), and the respective lifetimes (τ)[27−29] relevant for trADFRET calculation and the Förster distance (R_0). We also report the anisotropy (r_{ss}) values of the dyes attached by flexible linkers to the duplexes to calculate the dipole–dipole dye orientation factor ($\langle\kappa^2\rangle$) lower and upper values, $\langle\kappa^2\rangle_{min}$ and $\langle\kappa^2\rangle_{max}$, respectively (Database S2), to set the maximum and minimum interdye distances, R_{max} and R_{min}, in the case that $\langle k^2\rangle$ is different from 2/3 when the dye depolarization isotropy condition is not achieved.[30]

3.2. Traditional trDDFRET. We calculated trFRET-derived distance distribution ($P(R)$) that has a mean distance, $\overline{R}$, and a standard deviation (σ) for the double-labeled 14 N' and 29 N' oligos, using both traditional trDDFRET (Figure 2A–D)[29] and trADFRET (Figure 2E–N). In the case of the former, the D intensities of 14 N' (orange, I_D) and D in the presence of the A (green, $I_{D(A)}$) were collected with a 520-nm interference filter for the LaserStrobe (Figure 2A) and FluoTime (Figure 2B, Database S3). Thus, the deconvoluted 14 N' I_D and $I_{D(A)}$ yielded the lifetime (Database S3) difference, $\Delta\tau = \tau_D - \tau_{D(A)}$, this difference is caused by the energy transfer process which provides information to calculate the $P(R)$'s $\overline{R}$ and σ values (eq 3

https://dx.doi.org/10.1021/acs.analchem.0c04492
Anal. Chem. 2021, 93, 4841−4849

Table 2. Calculated Inter-Dye Distances Acquired by trDDFRET and trADFRET for the *N′* Series

			14*N′*		29 *N′*	
instrumentation	methodology	equation[d]	$\overline{R}$ (Å)	σ (Å)	$\overline{R}$ (Å)	σ (Å)
LaserStrobe	trDDFRET[a]	3	64.5 ± 1.8	7.1 ± 0.2	NA	NA
	trADFRET[b]	18	64.3 ± 1.1	5.3 ± 0.7	117.4 ± 1.9	4.0 ± 0.3
FluoTime	trDDFRET[a]	3	63.1 ± 1.9	8.5 ± 0.9	NA	NA
	trADFRET[c]	18	63.3 ± 1.1	5.0 ± 0.9	115.9 ± 2.4	15.2 ± 1.9
		average	63.8 ± 1.5	6.5 ± 1.6	116.6 ± 2.1	9.6 ± 7.9

[a]Database S4. [b]Database S5. [c]Database S6. [d]Values are calculated by simplex minimization routines, and the errors correspond to the standard deviation of the univariate analysis for each parameter[29] assuming a $\langle k^2 \rangle = 2/3$ under the isotropic condition where all dye dipole orientations are present at the energy transfer process, resulting in the $\overline{R}$ value. We used long flexible linkers to tether our dye probes to the duplex DNA to maximize the possibility of the isotropic state. However, when dye isotropic conditions are not attained, there is larger uncertainty in calculating the interdye distances, which can be estimated as an R_{max} and R_{min} range by finding the upper and lower bounds of $\langle k^2 \rangle$ by employing anisotropy depolarization information (Database S2). For the 5′- Xr*DNA$_{ds}$ and DNA$_{ds}$*Fl end-labeled duplexes (*N′* series), the $\langle k^2 \rangle_{max}$ and $\langle k^2 \rangle_{min}$ were 1.787 and 0.341 respectively, and these $\langle k^2 \rangle$ bounds were calculated according to Dale et al.[30] which yielded an R_{max} of +19% and R_{min} of −11% of the reported $\overline{R}$.

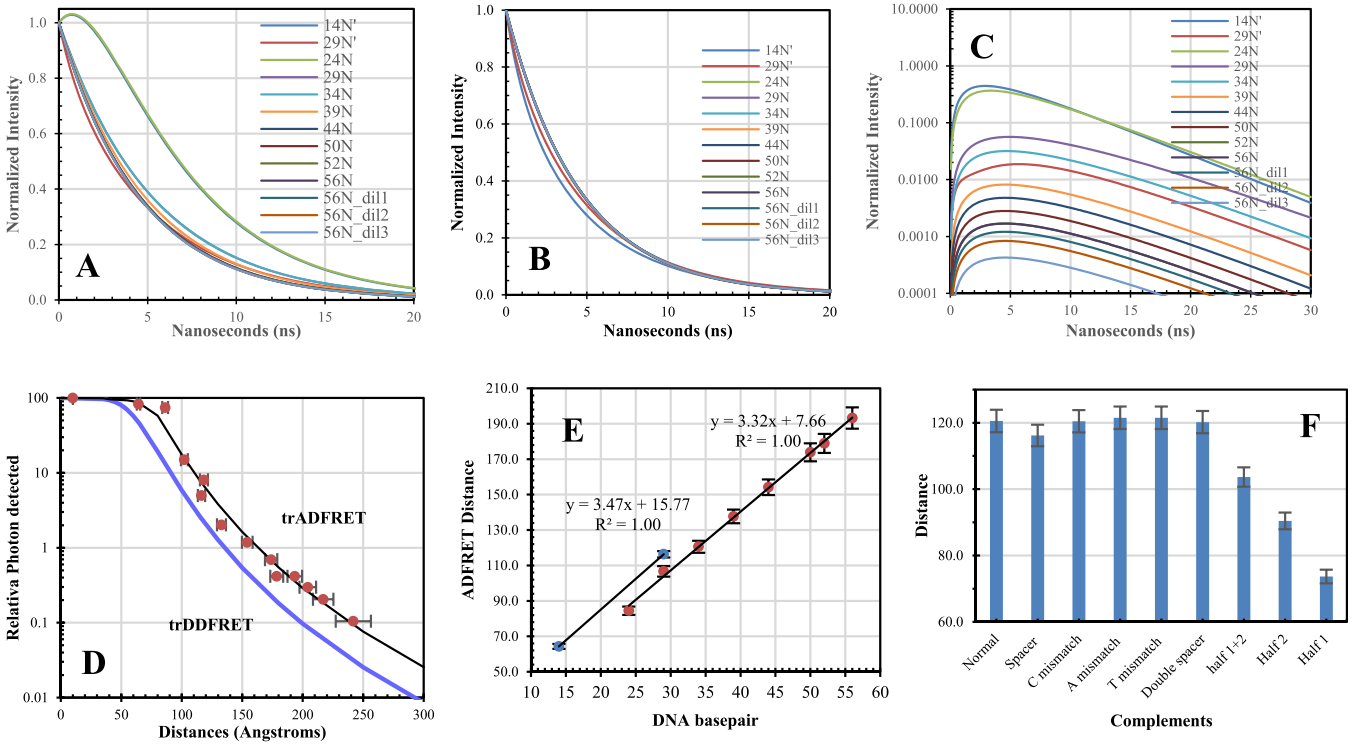

Figure 3. Time-resolved ADFRET. (A) Deconvoluted $\tau^{Obs}_{trADFRET}$ for the *N′* and *N* series (Database S12). (B) Each oligo has a respective $\langle \tau_{Std} \rangle$, which contains deconvoluted τ_D and τ_A under no FRET conditions, at an "*r*" ratio. The $\langle \tau_{Std} \rangle$ needs to be removed from $\tau^{Obs}_{trADFRET}$ (figure A minus figure B) to yield the sensitized $I_{trADFRET}$, which is fitted to obtain the $\overline{R}$ and σ (eq 18) and $^{tr}R_{SS}$ (eq 29) (C). (D) The trADFRET integration values as a function of $\overline{R}$ have ∼3-fold more photons collected than trDDFRET since the former accumulates signal over the $\langle \tau_{Std} \rangle$, and in contrast to the $\tau_{D(A)}$ of trDDFRET that cannot get higher than τ_D thus acting as a top limit (blue, 2D). (E) The trADFRET plot of $^{tr}R_{SS}$ (Eq 29) vs basepairs for the *N′* (blue, eq 30) and *N* (brown eq 29) oligo series (Database S12) were fitted to lines whose slopes corresponded to the nucleotide rise of 3.5 ± 0.1 Å and 3.3 ± 0.1 Å, respectively, which are in excellent accord with predictions for B-DNA.[33] Also, the intercepts yielded the length of linkers toward the dyes′ dipole moment with values of 15.8 ± 4.4 Å and 7.7 ± 2.4 Å, respectively. (F) The 34 N trADFRET $^{tr}R_{SS}$ acquired with a standard complement and several complements with noncanonical basepairs; such as, A, C, T, and an abasic spacer at position 17, and double abasic spacers at 17 and 18 positions, complement fragments divided into two halves, which were added separately (half1 or half2) or collectively (half1 + half2) (Database S12).

supplementary text, Table 2, Database S4). While in the case of the 29 *N′*, the $\Delta\tau$ values (Database S3) were 0.105 ns (± 0.044 ns) and −0.041 ns (± 0.022 ns), for LaserStrobe and FluoTime, respectively, which overlapping impedes the $P(R)$ determination (Table 2, Figure 2C,D, Database S4).

3.3. The trADFRET Mathematical Treatment. All relevant equations are addressed in the supplementary text materials. The trADFRET observed intensity acquired by the 620-nm interference filter, $S^{Exc/620nm}_{trADFRET}(t)$ (eq 8) and whose deconvolution yields $\tau^{Obs}_{trADFRET}$, contains three signals, the sensitized ADFRET (I_{ADFRET}), the leaked D(A) ($I_{D(A)}$), and directly excited A intensities (I_A) for the LaserStrobe (Figure 2E-I, Database S5) and FluoTime (Figure 2J−N, Database S6). The last two ($I_{D(A)} + I_A$) must be eliminated to observe the sensitized $I_{trADFRET}$ whose kinetic feature is strikingly different in the time course (Figure 2G,L), compared to trDDFRET (Figure 2A−D) since it rises from zero to a maximum amplitude (*Gain*) at a maximum time (t_{max}) as the excited D* transfers energy to pump

https://dx.doi.org/10.1021/acs.analchem.0c04492
Anal. Chem. 2021, 93, 4841−4849

Table 3. Simplified trADFRET Inter-Dye Distance $^{tr}R_{SS}$

oligo[a]	$\tau^{Obs}_{trADFRET}$, (ns)[b]	$\langle\tau_{Std}\rangle$ (ns)	$\langle\tau_{Diff}\rangle$ (ns)	"r" ratio[c]	gain	signal/noise[d]	$^{tr}R_{SS}$[e] (Å)
29 N′ (LaserStrobe)	4.644	4.423	0.220	1.891	2.523	0.8	119.1
	(± 0.013)	(± 0.166)	(± 0.087)	(± 0.065)	(± 0.100)	(± 0.3)	(± 8.6)
29 N′ (FluoTime)	4.991	4.729	0.262	3.433	2.785	18.4	117.6
	(± 0.014)	(± 0.001)	(± 0.003)	(±0.292)	(± 0.185)	(± 0.2)	(± 3.3)
24 N (FluoTime)	7.245	4.553	2.691	0.662	4.298	35.889	86.3
	(± 0.074)	(± 0.001)	(± 0.010)	(± 0.016)	(± 1.296)	(± 0.393)	(± 2.4)
29 N (FluoTime)	5.529	4.553	0.976	0.662	4.298	217.911	102.2
	(± 0.004)	(± 0.001)	(± 0.001)	(±0.016)	(± 1.296)	(± 0.257)	(± 2.8)
34 N (FluoTime)	4.958	4.553	0.404	0.662	4.298	58.314	118.3
	(± 0.007)	(± 0.001)	(± 0.001)	(±0.016)	(± 1.296)	(± 0.216)	(± 3.3)
39 N (FluoTime)	4.662	4.493	0.169	0.523	3.705	18.268	132.8
	(± 0.009)	(± 0.001)	(± 0.002)	(± 0.013)	(± 1.116)	(± 0.214)	(± 3.7)
44 N (FluoTime)	4.605	4.528	0.077	0.600	4.048	5.649	154.1
	(± 0.013)	(± 0.001)	(± 0.003)	(± 0.015)	(± 1.220)	(±0.213)	(± 4.4)
50 N (FluoTime)	4.585	4.528	0.039	0.643	4.221	4.102	173.9
	(± 0.009)	(± 0.001)	(± 0.002)	(± 0.016)	(± 1.273)	(± 0.214)	(± 5.1)
52 N (FluoTime)	4.584	4.550	0.034	0.654	4.265	4.378	178.5
	(± 0.007)	(± 0.001)	(± 0.002)	(± 0.016)	(± 1.286)	(± 0.287)	(± 5.3)
56 N (FluoTime)	4.565	4.544	0.021	0.640	4.209	4.865	193.4
	(± 0.004)	(± 0.007)	(± 0.002)	(± 0.016)	(± 1.269)	(± 0.407)	(± 6.0)
56 N[f] (+1/3f) (FluoTime)	4.559	4.544	0.015	0.640	4.209	3.883	213.1
	(± 0.004)	(± 0.007)	(± 0.002)	(± 0.016)	(± 1.269)	(± 0.438)	(± 6.9)
56N[f] (+2/3f) (FluoTime)	4.555	4.544	0.011	0.640	4.209	2.623	226.9
	(± 0.004)	(± 0.007)	(± 0.002)	(± 0.016)	(± 1.269)	(± 0.428)	(± 8.5)
56N[f] (+1f) (FluoTime)	4.550	4.544	0.006	0.640	4.209	1.266	254.3
	(± 0.004)	(± 0.007)	(± 0.002)	(± 0.016)	(± 1.269)	(± 0.405)	(± 14.6)

[a]See Table 1. The 14′*N* distance is better described by eq 18 (Database S6). The lifetime errors are the standard deviation of fits (Database S12). [b]The observed $\tau^{Obs}_{trADFRET}$ is the deconvoluted lifetime of $S^{Exc/620nm}_{trADFRET}(t)$ intensity collected at 620 nm at excitations of 470 and 481 nm for the FluoTime and LaserStrobe, respectively. [c]The *"r"* ratio is calculated according to Method a for each oligomer. [d]The signal-to-noise ratio (S/N)[35] was calculated according to: $S/N = \frac{\tau^{Obs}_{trADFRET} - \langle\tau_{std}\rangle}{\sqrt{\sigma^2_{\tau^{Obs}_{trADFRET}} + \sigma^2_{\langle\tau_{std}\rangle}}}$, where $\sigma^2_{\tau_{ADFRET}}$ and $\sigma^2_{\langle\tau_{std}\rangle}$ are variances of $\tau^{Obs}_{trADFRET}$ and $\langle\tau_{std}\rangle$, respectively. [e]The $^{tr}R_{SS}$ errors are calculated with propagation analysis (Database S11 and Database S12) assuming a $\langle k^2\rangle = 2/3$ at the isotropic condition in which all dye dipole orientations are present at the time of the energy transfer process. We used flexible linkers to tether our dye probes to the duplex DNA to maximize the isotropic state. However, when dye isotropic conditions are not attained, there is larger uncertainty in calculating the interdye distances, which can be estimated as upper and lower *R* values, R_{max} and R_{min}, respectively, by finding the upper and lower bounds of $\langle k^2\rangle$. For the 5′-Xr and Fl_{int} labeled probes (N series), the $\langle k^2\rangle_{max}$ and $\langle k^2\rangle_{min}$ were 1.611 and 0.375, respectively, and these values were calculated according to Dale et al.[30] with the dye anisotropy values of the Xr*DNA_{ds} and DNA_{ds}*Fl_{int} duplexes (Database S2). The resulted R_{max} and R_{min} were + 17 and −10% of the reported $\bar{R}$ at isotropic conditions. In the case of the 5′-Xr and 3′-Fl end-labeled duplexes (*N*′ series), the R_{max} and R_{min} were + 19 and −11%, respectively, for which the $\langle k^2\rangle_{max}$ and $\langle k^2\rangle_{min}$ were 1.787 and 0.341, respectively. [f]Standard-solution aliquots addition in terms of mole fraction (f) to the 56 N.

A to an excited state A* followed by subsequent τ_A decay. t_{max} is delayed as the inter-dye separation increases as observed from 14 *N*′ to the 29 *N*′ since the k_t decreases and t_{max} takes a longer time to build up a maximum A* concentration (Figure 2H,I,M,N).

We elucidated three methodologies to find the $I_{D(A)}/I_A$ ratio or *"r"* value for each of the *N*′ and *N* series (Supporting Information; Method a, Figure S2, Database S7; Method b, Figure S3, Database S8; and Method c, Figure S4, Table S1, Database S9). For the former, the *"r"* values were 1.891 ± 0.066 and 3.433 ± 0.292 for the LaserStrobe and FluoTime (Table S2, Database S9), and these values impact the *Gain* values which were 2.524 ± 0.046 (Database S5) and 2.785 ± 0.091 (Database S6), respectively since the excitation and photon detection systems are not the same. Notably, the 14 *N*′ *P*(*R*) values calculated with trDDFRET (Figure 2A,B) and trADFRET are statistically indistinguishable (Table 2, Database S5, and Database S6), thus validating our novel approach. As anticipated, the 29 *N*′ trDDFRET did not provide distance information (Figure 2C,D); however, we obtained the trADFRET *P*(*R*) (Eq 18) despite that energy transfer was 2.35% (Table 2, Database S1).

3.4. Time-Resolved ADFRET Simplification. At inter-dye distances of 100−120 Å, t_{max} converges while *Gain* steadily declines and is highly correlated with the *P*(*R*) parameters, which complicates the determination of ^{-}R and σ (Table 2, Figure S5, Database S10). Therefore, we sought to simplify the calculation by setting the *P*(*R*) integration equal to 1 (Eq 18) resulting in a novel equation that yields a time-resolved derived distance, $^{tr}R_{SS}$ that in principle equates to a steady-state (ss) measurement (Eq 29 and Eq 30). Remarkably, the 29 *N*′ $^{tr}R_{SS}$ values for the LaserStrobe and FluoTime were 119.1 ± 8.6 Å and 117.6 ± 3.3 Å, overlapping in the error, with S/N ratios of 0.8 ± 0.3 and 18.4 ± 02, respectively. The difference in S/N is expected since the FluoTime has higher collection rates than LaserStrobe (Database S11).

3.5. Long trADFRET Interactions. The $\langle\tau_{Std}\rangle$ values can be subtracted from $\tau^{Obs}_{trADFRET}$ (Figure 3A,B) to yield the sensitized $I_{trADFRET}$ whose integration is the number of trADFRET photons collected (Figure 3C) that at the current experimental settings

https://dx.doi.org/10.1021/acs.analchem.0c04492
Anal. Chem. 2021, 93, 4841−4849

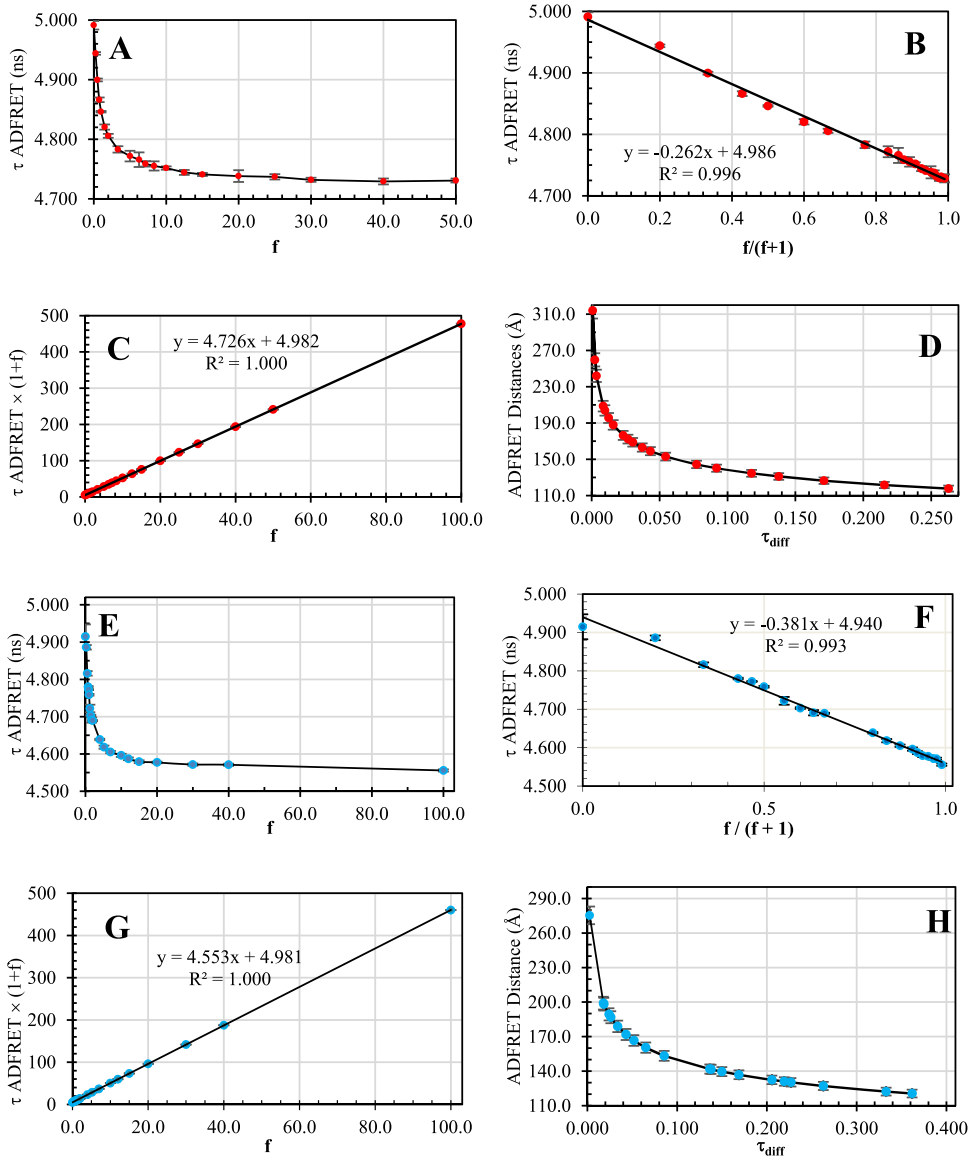

Figure 4. Time-resolved ADFRET limits of each series were found by adding aliquots of the standard mixture solution, in molar basics (f), to simulate FRET at longer $\bar{R}$ as the observed $S_{trADFRET}$ is being overwhelmed by a stronger background intensity. (A) For the 29 N', the $\tau^{Obs}_{trADFRET}$ dynamic range was 4.991 ± 0.007 ns to 4.729 ± 0.005 ns from 0 f to 40 f (standard solution), respectively, and further aliquot addition did not result in $\tau^{Obs}_{trADFRET}$ change (Database S13). (B) The $\tau^{Obs}_{trADFRET}$ vs normalized dilution factor, $f/(f+1)$, yielded a line with a slope (m = −0.262 ns ± 0.018 ns) that corresponds to the dynamic range. The intercept (b = 4.986 ns ± 0.014 ns) is the initial $\tau^{Obs}_{trADFRET}$ of the 29 N′. (C) The $\tau^{Obs}_{trADFRET} \times (1+f)$ vs f plot yielded a straight line with a slope that corresponds to $\langle\tau_{Std}\rangle$ = 4.726 ns ± 0.001 ns, and the intercept (b = 4.982 ns ± 0.042 ns) yielded also the initial $\tau^{Obs}_{trADFRET}$. (D) The corresponding 29 N $^{tr}R_{SS}$ was 117.7 Å ± 3.3 Å (S/N = 35.9 ± 0.2) and 242 ± 6.8 Å (S/N = 0.92 ± 0.20) for the last dilution. (E) A similar approach was carried out for 34 N, which resulted in a dynamic range of 4.915 ± 0.032 ns to 4.553 ± 0.011 ns from 0 f to 100 f, respectively (Database S14). (F) The $\tau^{Obs}_{trADFRET}$ vs normalized dilution factor, $f/(f+1)$, yielded a line with a slope (m = −0.381 ± 0.008 ns) that corresponds to the dynamic range, and the intercept (b = 4.940 ± 0.006 ns) was the initial $\tau^{Obs}_{trADFRET}$ for the 34 N. (G) The $\tau^{Obs}_{trADFRET} \times (1+f)$ vs f plot yielded a straight line with a slope that corresponded to $\langle\tau_{Std}\rangle$= 4.553 ± 0.001 ns, and the intercept (b = 4.984 ± 0.025 ns) yielded also the initial $\tau^{Obs}_{trADFRET}$. (H) The corresponding 34 N $^{tr}R_{SS}$ was 120.5 ± 3.4 Å (S/N = 11.1 ± 0.1) and 275.3 ± 7.7 Å (S/N = 0.85 ± 0.07) for the last dilution.

has ∼3-fold stronger signal than the trDDFRET signal, calculated by 100% × $(1 - \tau_D/\tau_{D(A)})$ (Figure 3D). Consequently, the trADFRET acquisition regime is analogous to the NMR[31] and MRI[32] accumulation principles as the sensitized trADFRET signal stack up from a steady reference like adding icing to a cake in multiple layers. In contrast, the trDDFRET cannot be beneficiated from this method since the $\tau_{D(A)}$ approaches toward the reference τ_D, which acts as a limiting ceiling.

Accordingly, we successfully calculated the $^{tr}R_{SS}$ for both oligo series (Table 3, Database S12) with the smallest value of 84.4 ± 2.4 Å and the longest of 193.2 ± 6.0 Å for the 24 N and 56 N duplexes, respectively (Figure 3E). The N series plot of $^{tr}R_{SS}$ values vs the number of nucleotides (Figure 3E) resulted in a slope of 3.3 ± 0.1 Å, which is in excellent agreement with the nucleotide increase observed in crystallographic studies.[33] The intercept yielded a length of the linkers and dyes of 7.7 ± 2.4 Å. In the case of the N′ series, the slope was 3.5 ± 0.2 Å and the intercept was 15.8 ± 4.4 Å (Database S12). The intercepts were not similar for these two series since the 3′Fl-linker is extended outward, and the Fl_{int}-linker is perpendicular to the duplex (Figure 3E). Interestingly, at these longer distances, we did not

https://dx.doi.org/10.1021/acs.analchem.0c04492
Anal. Chem. 2021, 93, 4841−4849

observe the helicity of B-DNA since the linkers are long and bring the dyes to the water environment and away from the DNA structure, further justifying a $\kappa^2 = 0.667 \pm 0.083$ (Database S2). However, the helicity can be observed when the dyes are sitting with very short linkers on the end termini in shorter duplexes, 10, and 24 nucleotides.[34]

Also, we have calculated the 34 N $^{tr}R_{SS}$ values (eq 29) hybridized with standard and noncanonical complements (Figure 3F, Database S12). The 34 *N* distance was ~120.5 ± 3.4 Å, which was not possible to detect by trDDFRET. In contrast, we observed a shorter $^{tr}R_{SS}$ value of 103.7 ± 2.9 Å when the 34 *N* duplex was hybridized with two complement halves, non-interconnected with respect to the canonical complement since a kink is formed between nucleotide 19 and 20 of the top stand. In contrast, when only the left- and the right-half fragments were hybridized the $^{tr}R_{SS}$ values were 90.4 ± 2.5 Å, and 73.7 ± 2.1 Å, respectively (Figure 3F, Database S12) since for each case the overhangs are not straight.

3.6. Time-Resolved ADFRET Limits. We designed an experiment to mask and overwhelm the sensitized I_{ADFRET} to determine the upper limit by adding aliquots (f) of the standard solution, made of a mix of 1:1 single-labeled A and D duplexes, (Xr*DNA_{ds}, DNA_{ds}*Fl, or DNA_{ds}*Fl_{int}) that are not attached to the same DNA_{ds}, to its respective 29 *N*′ (Figure 4A, Database S13) and 34 *N* (Figure 4E, Database S14). By adding the (f) standard solution to the double-labeled duplex (29 *N*′ or 34 *N*) more donor and acceptor background (Figure 1B, yellow and red curves, respectively) that does not contain FRET distance information is detected with respect to the distance-containing information of I_{ADFRET}". Indeed, the $\tau^{Obs}_{trADFRET}$ plotted as a function of normalized aliquot, $f/(f+1)$, was fitted to a line with a slope "m" that yielded the dynamic range for both series, and the intercept "b" corresponded to the initial $\tau^{Obs}_{trADFRET}$ (Figure 4B,F). Similarly, the plot of $\tau^{Obs}_{trADFRET} \times (1+f)$ vs f, was fitted to a line whose slope was equal to $\langle\tau_{Std}\rangle$ and the intercept yielded the initial optimal $\tau^{Obs}_{trADFRET}$ for the 29 *N*′ (Figure 4C) and 34 N (Figure 4G). The maximum $^{tr}R_{SS}$ for the 29 *N*′ and 34 *N* masking experiments were 242.0 ± 6.8 Å (Figure 4D, Database S13) and 275.3 ± 7.7 Å (Figure 4H, Database S14), whose S/N ratios were 0.92 ± 0.20 and 0.85 ± 0.07, and FRET efficiencies were 0.028 and 0.013% (Database S1), respectively.

4. CONCLUSIONS

Our FLIM-trADFRET technique allows distance calculations up to ~275 Å, an approximately threefold improvement over traditional trDDFRET. To achieve success, we have accomplished the following: (1) developing the trADFRET requisite equations; (2) simplifying the trADFRET analysis to obtain a single $^{tr}R_{SS}$ value; (3) devising dependable experimental methods to extract the sensitized $I_{trADFRET}$ that self-corrects for any dye ratio; (4) understanding clearly how to account for leaked $I_{D(A)}$ and direct excited I_A through the parameter "*r*" ratio; and (5) lastly, determining the relevant dye spectroscopic parameters that impact trADFRET.

The FLIM-trADFRET technology will be able to monitor macromolecular assemblies (Figure 1) since they are responsible for the most relevant functions for life, such as replication, transcription, translation, vesicular transport, and viral and parasitic infection. A detailed understanding of these macromolecular mechanisms in diseased and healthy tissue can result in new therapies to stop cancer,[36] fight malaria,[37] HIV,[38] or even SARS-CoV19,[39] as discussed by Dr. Stephan Hell, Dr. William Moerner, and Dr. Eric Betzig at the Nobel Prize talk in 2014.[40−48]

■ ASSOCIATED CONTENT

Supporting Information

The Supporting Information is available free of charge at https://pubs.acs.org/doi/10.1021/acs.analchem.0c04492.

FLIM-trADFRET mathematical analysis, structure of the double-labeled N′ oligos, standard mixture preparation and "r" ratio by Method a, the "r" value calculated by Method b and Method c, gain, and t_{max} dependence for sensitized $I_{trADFRET}$ as a function of $\bar{R}$ and σ, the "r" ratio was acquired with "Method c" for both series, and, The "r" ratio of the three methodologies for N′ series and the respective crosstalking $I_A/I_{D(A)}$ ratio of leaked intensities (PDF)

DatabaseS1_(trADFRET_and_trDDFRET_simulations) (XLSX)

DatabaseS2_(R0_anisotropy_kappasquared) (XLSX)

DatabaseS3_(trDDFRET_Lifetime_both_instruments) (XLSX)

DatabaseS4_(trDDFRET_fits_both_instruments) (XLSX)

DatabaseS5_(trADFRET_LaserStrobe) (XLSX)

DatabaseS6_(trADFRET_FluoTime_Table2) (XLSX)

DatabaseS7_(FigS2_r_value_Method_a) (XLSX)

DatabaseS8_(FigS3_Method_b) (XLSX)

DatabaseS9_(FigS4_r_value_Method_c) (XLSX)

DatabaseS10_(FigS5_P(R)_and_Gain_correlation) (XLSX)

DatabaseS11_trRss(eqn30)_and_signal-noise (XLSX)

DatabaseS12_trRss_Nseries_and_Table2 (XLSX)

DatabaseS13_Limit_dilution_N′series (XLSX)

DatabaseS14_Limit_dilution_Nseries (XLSX)

■ AUTHOR INFORMATION

Corresponding Authors

Roberto F. Delgadillo − *Department of Chemistry, University of Nebraska - Lincoln, Lincoln, Nebraska 68588-0304, United States; Tecnologico de Monterrey, School of Engineering and Sciences, Nuevo Leon 64849 Monterrey, Mexico; BASF Enzymes LLC, San Diego, California 92121, United States;* orcid.org/0000-0002-5743-9781; Email: delgadillo@tec.mx

Lawrence J. Parkhurst − *Department of Chemistry, University of Nebraska - Lincoln, Lincoln, Nebraska 68588-0304, United States*; Email: lparkhurst1@unl.edu

Authors

Katie A. Carnes − *GlaxoSmithKline, Medicinal Science and Technology, CMC Analytical − Drug Substance and Product Analysis, King of Prussia, Pennsylvania 19406, United States*

Kathia Zaleta-Rivera − *Department of Bioengineering, University of California San Diego, San Diego, California 92093-0412, United States*

Omar Olmos − *Tecnologico de Monterrey, School of Engineering and Sciences, Nuevo Leon 64849 Monterrey, Mexico*

Complete contact information is available at: https://pubs.acs.org/10.1021/acs.analchem.0c04492

https://dx.doi.org/10.1021/acs.analchem.0c04492
Anal. Chem. 2021, 93, 4841−4849

Author Contributions

Conceptualization: R.F.D., L.J.P. Data curation: R.F.D. Formal analysis: R.F.D. Funding acquisition: R.F.D., O.O., L.J.P. Investigation: R.F.D. Methodology: R.F.D., L.J.P. Project administration: R.F.D., L.J.P. Resources: R.F.D., L.J.P. Software: R.F.D., L.J.P. Supervision: R.F.D., K.Z.R., K.A.C., L.J.P. Validation: R.F.D., K.Z.R., K.A.C., L.J.P. Visualization: R.F.D. Writing – original draft: R.F.D. Writing – review & editing: R.F.D., K.A.C., K.Z.R., L.J.P.

Notes

The authors declare no competing financial interest.

The work was supported by National Institutes of Health Grants GM59346 and RR015468 to LJP; CONACYT-Mexico postdoctoral, SNI fellowships (130994,162809, SNI75487), and the Government of Veracruz-Mexico fellowships to R.F.D. All data is available in the main text or the supplementary materials.

■ ACKNOWLEDGMENTS

We wish to thank Prof. R. S. Knox for helpful discussions concerning the refractive index. We thank Dr. Justin W. Shearer, Dr. Efrain Soto Apolinar, Dr. Blas Rodriguez, Ms. Carolina Flores-Ballesteros, and Ms. Alethia D. Guzman for proofreading the manuscript.

■ REFERENCES

(1) Balzarotti, F.; Eilers, Y.; Gwosch, K. C.; Gynnå, A. H.; Westphal, V.; Stefani, F. D.; Elf, J.; Hell, S. W. *Science (80-)* **2017**, *355*, 606−612.
(2) Rudkouskaya, A.; Sinsuebphon, N.; Intes, X.; Mazurkiewicz, J. E.; Barroso, M. *Multiphot. Microsc. Biomed. Sci. XVII* **2017**, *10069*, No. 1006917.
(3) Suhling, K.; Hirvonen, L. M.; Levitt, J. A.; Chung, P.-H.; Tregidgo, C.; Le Marois, A.; Rusakov, D. A.; Zheng, K.; Ameer-Beg, S.; Poland, S.; et al. *Med. Photonics* **2015**, *27*, 3−40.
(4) Jinek, M.; Chylinski, K.; Fonfara, I.; Hauer, M.; Doudna, J. A.; Charpentier, E. *Science (80-)* **2012**, *337*, 816−821.
(5) Yamanaka, M.; Smith, N. I.; Fujita, K. *Microscopy* **2014**, *63*, 177−192.
(6) Gelles, J.; Schnapp, B. J.; Sheetz, M. P. *Nature* **1988**, *331*, 450−453.
(7) Mali, P.; Yang, L.; Esvelt, K. M.; Aach, J.; Guell, M.; DiCarlo, J. E.; Norville, J. E.; Church, G. M. *Science (80-)* **2013**, *339*, 823−826.
(8) Cong, L.; Ran, F. A.; Cox, D.; Lin, S.; Barretto, R.; Habib, N.; Hsu, P. D.; Wu, X.; Jiang, W.; Marraffini, L. A.; et al. *Science (80-.)* **2013**, *339*, 819−823.
(9) Kyrychenko, A.; Rodnin, M. V.; Ghatak, C.; Ladokhin, A. S. *Anal. Biochem.* **2017**, *522*, 1−9.
(10) Grossman, S. H. *Biochemistry* **1989**, *28*, 4894−4902.
(11) Gordon, G. W.; Berry, G.; Liang, X. H.; Levine, B.; Herman, B. *Biophys. J.* **1998**, *74*, 2702−2713.
(12) Zal, T.; Gascoigne, N. R. J. *Biophys. J.* **2004**, *86*, 3923−3939.
(13) Raicu, V.; Jansma, D. B.; Miller, R. J.; Friesen, J. D. *Biochem. J.* **2005**, *385*, 265−277.
(14) Chang, C.; Sud, D.; Mycek, M. *Methods Cell Biol.* **2007**, *81*, 495−524.
(15) Clegg, R. M. *Methods Enzymol* **1992**, *211*, 353−388.
(16) Delgadillo, R. F.; Carnes, K. A.; Valles-Villarreal, N.; Olmos, O.; Zaleta-Rivera, K.; Parkhurst, L. J. *Biosensors* **2020**, *10*, No. 180.
(17) Sijbers, J.; Scheunders, P.; Bonnet, N.; Van Dyck, D.; Raman, E. *Magn. Reson. Imaging* **1996**, *14*, 1157−1163.
(18) Gruetter, R.; Adriany, G.; Choi, I.-Y.; Henry, P.-G.; Lei, H.; Öz, G. *NMR Biomed.* **2003**, *16*, 313−338.
(19) Maher, E. A.; Marin-Valencia, I.; Bachoo, R. M.; Mashimo, T.; Raisanen, J.; Hatanpaa, K. J.; Jindal, A.; Jeffrey, F. M.; Choi, C.; Madden, C.; et al. *NMR Biomed.* **2012**, *25*, 1234−1244.
(20) Lauterbur, P. C. *Nat. (London, United Kingdom)* **1973**, *242*, 190−191.
(21) Plewes, D. B.; Kucharczyk, W. *J. Magn. Reson. Imaging* **2012**, *35*, 1038−1054.
(22) Damadian, R. *Science (80-)* **1971**, *171*, 1151−1153.
(23) Finley, J. A. Us7889118. US 7,889,118 B1, 2011.
(24) Packer, M. J.; Dauncey, M. P.; Hunter, C. A. *J. Mol. Biol.* **2000**, *295*, 71−83.
(25) Packer, M. J.; Dauncey, M. P.; Hunter, C. A. *J. Mol. Biol.* **2000**, *295*, 85−103.
(26) Edelhoch, H.; Brand, L.; Wilchek, M. *BioChemistry* **1968**, *7*, 3893−3900.
(27) Delgadillo, R. F.; Parkhurst, L. J. *Photochem. Photobiol.* **2010**, *86*, 261−272.
(28) Vogel, S. S.; Nguyen, T. A.; van der Meer, B. W.; Blank, P. S. *PLoS One* **2012**, *7*, No. e49593.
(29) Delgadillo, R. F.; Whittington, J. D. E.; Parkhurst, L. K.; Parkhurst, L. J. *Biochemistry* **2009**, *48*, 1801−1809.
(30) Dale, R. E.; Eisinger, J.; Blumberg, W. E. *Biophys. J.* **1979**, *26*, 161−193.
(31) Bloch, F.; Hansen, W. W.; Packard, M. *Phys. Rev.* **1946**, *70*, 474−485.
(32) Lauterbur, P. C. *Nature* **1973**, *242*, 190−191.
(33) Watson, J. D.; Crick, F. H. C. *Nature* **1953**, *171*, 737.
(34) Iqbal, A.; Arslan, S.; Okumus, B.; Wilson, T. J.; Giraud, G.; Norman, D. G.; Ha, T.; Lilley, D. M. J. *Proc. Natl. Acad. Sci. U. S. A.* **2008**, *105*, 11176−11181.
(35) Welvaert, M.; Rosseel, Y. *PLoS One* **2013**, *8*, No. e77089.
(36) Rothman, J. E. *Nat. Med.* **2002**, *8*, 1059−1062.
(37) Tu, Y. *Nat. Med.* **2011**, *17*, 1217−1220.
(38) Barre-Sinoussi, F. *J. Infect. Dis.* **2014**, *210*, S605.
(39) Wrapp, D.; Wang, N.; Corbett, K. S.; Goldsmith, J. A.; Hsieh, C.-L.; Abiona, O.; Graham, B. S.; McLellan, J. S. *Science* **2020**, *367*, 1260−1263.
(40) Möckl, L.; Lamb, D. C.; Bräuchle, C. *Moerner. Angew. Chemie Int. Ed.* **2014**, *53*, 13972−13977.
(41) Cantor, C.; Schimmel, P. *Biophysical Chemistry Part II: Techniques for the Study of Biological Structure and Function*; W.H. Freeman and Company: New York, 1980.
(42) Algar, W. R.; Hildebrandt, N.; Vogel, S. S.; Medintz, I. L. *Nat. Methods* **2019**, *16*, 815−829.
(43) Lakowicz, J. R. *Principles of Fluorescence Spectroscopy*, 3rd ed.; Springer: New York, 2006.
(44) Knox, R. S.; Van Amerongen, H. *J. Phys. Chem. B* **2002**, *106*, 5289−5293.
(45) Hardwidge, P. R.; Wu, J.; Williams, S. L.; Parkhurst, K. M.; Parkhurst, L. J.; Maher, L. J. *Biochemistry* **2002**, *41*, 7732−7742.
(46) Clegg, R. M.; Murchie, A. I.; Zechel, A.; Lilley, D. M. *Proc. Natl. Acad. Sci.* **1993**, *90*, 2994−2998.
(47) Berney, C.; Danuser, G. *Biophys. J.* **2003**, *84*, 3992−4010.
(48) (48) Delgadillo, R. F. Acceptor Detected Fluorescence Resonance Energy Transfer for Measurement up to 250 A and Biophysical Studies on Core TATA Binding Protein-DNA Complex. Ph.D. Dissertation, University of Nebraska-Lincoln: Lincoln, NE, USA, 2009. http://digitalcommons.unl.edu/dissertations/AAI3388957/ (accessed 2020-10-23)

■ NOTE ADDED AFTER ASAP PUBLICATION

This paper was originally published ASAP on March 10, 2021. Due to a production error, a black box was present in the TOC graphic. The corrected version was reposted on March 11, 2021.

https://dx.doi.org/10.1021/acs.analchem.0c04492
Anal. Chem. 2021, 93, 4841−4849